ELSEVIED

Contents lists available at ScienceDirect

Science of the Total Environment

journal homepage: www.elsevier.com/locate/scitotenv



Thermal air oxidation changes surface and adsorptive properties of black carbon (char/biochar)



Feng Xiao ^{a,*}, Alemayehu H. Bedane ^a, Julia Xiaojun Zhao ^b, Michael D. Mann ^c, Joseph J. Pignatello ^d

- ^a Department of Civil Engineering, University of North Dakota, Grand Forks, ND 58202-8115, United States
- ^b Department of Chemistry, University of North Dakota, Grand Forks, ND 58202-9024, United States
- ^c Department of Chemical Engineering, University of North Dakota, Grand Forks, ND 58202-7101, United States
- d Department of Environmental Sciences, Connecticut Agricultural Experiment Station, New Haven, CT 06504-1106, United States

HIGHLIGHTS

- Black carbon (BC) made by thermal air pyrolysis had underdeveloped pore structure.
- Substantial changes were observed by post-pyrolysis thermal air oxidation (AO).
- High-HTT BC showed significant increases in porosity and adsorptivity.
- Low-HTT BC showed moderate increases in these properties after thermal AO.
- Low-HTT BC showed an increase in surface oxygen functionality after thermal AO.

ARTICLE INFO

Article history:
Received 5 September 2017
Received in revised form 31 October 2017
Accepted 1 November 2017
Available online 10 November 2017

Editor: Jay Gan

Keywords:
Black carbon
Biochar
Carbon sequestration
Porosity enhancement
Polar functional groups
Environmental sustainability

GRAPHICAL ABSTRACT

Generation of surface oxygen functionality on low-HTT black carbon low-HTT black carbon char/biochar) Surface area and porosity enhancement Black carbon (char/biochar) Surface becomes more negatively charged

Thermal Air Oxidation of Black Carbon



ABSTRACT

In this study, we systematically investigated the effects of thermal air oxidation on the properties of biomass-derived black carbon (BC) made at carbonization temperatures (HTTs) of 300–700 °C. BC produced by including air in the carbonization step was found to have a low surface area and underdeveloped pore structure. Substantial changes of BC were observed after post-pyrolysis thermal air oxidation (PPAO). Well-carbonized BC samples made anoxically at relatively high HTTs (600 and 700 °C) showed, after PPAO, significant increases in N₂ BET surface area (SA) (up to 700 times), porosity (<60 Å) (up to 95 times), and adsorptivity (up to 120 times) of neutral organic species including two triazine herbicides and one natural estrogen. Partially carbonized BC made at a lower HTT (300 or 400 °C) showed moderate increases in these properties after PPAO, but a large increase in the intensity of Fourier transform infrared spectroscopy bands corresponding to various oxygen-containing functional groups. Well-carbonized BC samples, on the other hand, were deficient in surface oxygen functionality even after the PPAO treatment. Adsorption of the test organic compounds on BC generally trended with BET SA when it was less than 300 m²/g, but BET SA was poorly predictive of adsorption when it was greater than 300 m²/g. Overall, our results suggest that thermal reactions between molecular oxygen and BC 1) increase surface oxygen functionality more effectively for low-HTT than for high-HTT BC samples; 2) increase SA and porosity (<60 Å) especially for high-HTT BC samples: and 3) create new adsorption sites and/or relieve steric restriction of organic molecules to micropores, thereby enhancing the adsorptivity of BC. These results will prove useful not only for understanding the fate of environmental BC but also in devising strategies for improving the practical performance of the engineered form of BC (i.e., biochar).

 $\hbox{@ 2017}$ Elsevier B.V. All rights reserved.

^{*} Corresponding author.

E-mail addresses: Feng.Xiao@engr.UND.edu, fxiaoee@gmail.com (F. Xiao).

1. Introduction

Black carbon is a collective term referring to the carbonaceous residue of combusted or pyrolyzed organic substances. It is widespread in soils and sediments (Schmidt et al., 2001; Czimczik and Masiello, 2007). A major source of environmental black carbon is biomass-derived char formed during natural wildfires and burning practices associated with land clearing and crop residue removal (Skjemstad et al., 1999; Schmidt and Noack, 2000; Skjemstad et al., 2002; Koelmans et al., 2006; Lehmann and Joseph, 2015). During thermal treatment, the lignocellulosic component of the biomass is converted to a porous char structure. Char is generally resistant to both abiotic and biotic degradation depending on the feedstocks and carbonization or pyrolysis temperature (Zimmerman, 2010; Spokas et al., 2014) and therefore represents a relatively long-term sink for carbon (Kuhlbusch and Crutzen, 1995; Glaser and Amelung, 2003). It can be dispersed in the environment by atmospheric circulation and surface runoff (Skjemstad et al., 1999: Schmidt and Noack, 2000: Skiemstad et al., 2002). In some soils, such as the Midwest prairie soils of the U.S., char carbon comprises up to 40-50% of total soil organic carbon (Glaser et al., 2001; Mao et al.,

Biochar, the engineered form of char, has recently attracted attention in the agro-environmental community for its promising beneficial effects as a soil amendment (Godlewska et al., 2017) for improving soil quality (Laird, 2008; Basso et al., 2012; Lehmann and Joseph, 2015), increasing crop productivity (Jeffery et al., 2011), suppressing nitrous oxide (an important greenhouse gas) emissions (Lehmann, 2007b; Woolf et al., 2010), and retaining metal (Cao et al., 2009; Uchimiya et al., 2012; Qian et al., 2013) and organic contaminants (Spokas et al., 2009; Graber et al., 2012; Graber and Kookana, 2015; Kupryianchyk et al., 2016; Kah et al., 2017; Stefaniuk et al., 2017; Zhu et al., 2017). Biochar is also believed to be a sustainable means of carbon sequestration (Woolf et al., 2010; Lehmann and Joseph, 2015). Recent studies have been performed to modify biochar or the carbonization process of biomass in order to enhance the desired properties of biochar (Rajapaksha et al., 2016). These modifications include addition of magnetic properties to biochar (Yang et al., 2016), conversion of biochar to a slow-release fertilizer (Yao et al., 2013), preparation of composites of biochar and nanoparticles (Inyang et al., 2014; Wang et al., 2017a), acid oxidation of biochar (Jin et al., 2017; Vu et al., 2017; Wu et al., 2017), and impregnation of biochar or its feedstock with metal oxides or minerals (Li et al., 2014).

This study introduces thermal air oxidation (AO) as a simple but effective approach to enhance the porosity and adsorptivity of biochar. This process is also very relevant to processes of black carbon formation and fate in soils. The functions and effects of black carbon are determined by surface properties, which, in turn, depend on formation conditions (Kloss et al., 2012; Ronsse et al., 2013). Native, fire-derived char is formed under a wide and fluctuating range of oxygen concentrations. Biochar is typically produced anoxically in order to maximize the yield, but air may be introduced during the process inadvertently or intentionally to reduce energy input (Marsh and Rodríguez-Reinoso, 2006; Gil-Lalaguna et al., 2014) or to cool the reactor (Mahinpey et al., 2009). Char or biochar in soils may also be exposed to hot air during subsequent wild fires, land clearing, or crop residue burning. From January 1 to October 6, 2017, there were approximately 50,283 wildfires in the United States that burned 8.5×10^6 acres (III, 2017). The effects of thermal AO on the properties of char/biochar left or discharged to soils and on the regional and global carbon cycles are potentially profound, but have not been well documented in the literature.

In a recent study (Xiao and Pignatello, 2016), it was found that postpyrolysis thermal AO (PPAO) of a maple wood char increased its porosity, surface area (SA), surface carboxyl group content, and adsorption of neutral and ionizable organic compounds. The authors proposed that hot oxygen during PPAO reamed pores by removing tarry materials from pores and etching pore walls, resulting in SA and porosity enhancement (Xiao and Pignatello, 2016). They also proposed that the introduced carboxyl groups enhanced adsorption of the ionizable compounds by providing strong charge-assistant hydrogen bonding sites. In that study, the maple wood char was made under inert atmosphere at a single heat treatment temperature (HTT) of 400 °C prior to PPAO at 400 °C in a second step (Xiao and Pignatello, 2016).

In the current study, we investigated the effects of PPAO on the properties of corncob-derived chars made at different HTTs ranging from 300 to 700 °C. The properties and functions of biochar/char depend on its feedstock and carbonization temperature (Lehmann and Joseph, 2015). Previous studies have shown that char made at a HTT of 300 °C is composed mainly of partially altered biomass residues, but char made at 400 °C or above loses most of its lignocellulosic features and consists mainly of polyaromatic structures (Keiluweit et al., 2010; Cao et al., 2012). The lignocellulosic and polyaromatic structures of char may respond differently to thermal air oxidation. In addition, the proportion of cellulose and lignin in the feedstock may be important. Corncob was selected as the feedstock in the present study because it is a common cellulose-rich agricultural residue with a lower lignin content than maple wood used in the previous study (Xiao and Pignatello, 2016) (15% versus 20-30% (Demirbas, 2004, Pointner et al., 2014, Faruk and Sain, 2016)). We also characterized char produced by direct air pyrolysis (AP) where air is present during carbonization. Oxidative pyrolysis has been studied as an approach for reducing the energy input while maximizing the yields of bio-oil and char from biomass (Senneca et al., 2002; Amutio et al., 2012). AP is relevant to the formation of chars in wildfires.

2. Materials and methods

Corncobs were dried in a forced air drying oven (Cascade Tek, Cornelius, OR) at 70 °C for >3 d, ground in a heavy-duty blender, and sieved. Corncob particles between 0.4 and 2 mm were used to produce char (referred as CB) by pyrolysis under a flow of N₂ (200 mL/min) at different heat treatment temperatures (HTTs) (300, 400, 500, 600 and 700 °C) in a dual zone tube furnace (MTI Corporation, CA). The chars were named CBxxx where xxx corresponds to the HTT (°C). The carbonization parameters were selected based on a previous study (Xiao and Pignatello, 2015a). Briefly, corncob particles were heated in the tube at 100 °C for 1 h. The temperature was then increased at a rate of 10 °C/min to the desired HTT at which the corncob particles were carbonized for 2 h, After carbonization, the furnace allowed to cool to 25 °C at 5 °C/min. The yield of CB was calculated on the basis of mass loss. PPAO treatment of CB particles was conducted at 400 °C (within the range of typical wildfire temperatures (Chandler et al., 1983)) in the manner described previously (Xiao and Pignatello, 2016). Briefly, 0.1 g CB particles in a cylindrical shaped aluminum foil tube were heated in a muffle furnace in an air atmosphere (Neytech., Vulcan 3-550, USA). In one experiment, CB samples were produced by heating corncob directly in the muffle furnace at 300 and 400 °C. This process is referred as AP (air pyrolysis). The burn-off of CB during PPAO or AP was calculated by:

$$Burnoff \ (wt.\%) = \left(\frac{W_{char/comcob} - W_{char,PPAO/AP}}{W_{char/comcob}}\right) \times 100\%, \tag{1}$$

where $W_{\rm char,PPAO/AP}$ is the weight of the original char or corncob and $W_{\rm char,PPAO/AP}$ is the weight of char produced by PPAO of char or AP of corncob.

The porosity and pore size distribution of CB particles were measured by means of N_2 porosimetry at 77 K (Autosorb-iQ, Quantachrome, Boynton Beach, FL). Before the measurement, the char sample was outgassed at 493 K under vacuum. The specific SA of char was calculated by the 11-point Brunauer–Emmett–Teller (BET) method. The microand meso-porosities and pore size distributions of char were determined by quenched solid density functional theory (QSDFT) from the N_2 adsorption isotherm at 77 K. QSDFT is a state-of-the-art DFT method

for pore size analysis that takes into account the effects of surface roughness and heterogeneity (Neimark et al., 2009). It should be noted that $\rm N_2$ porosimetry at 77 K may underestimate microporosity because of the retarded diffusion of $\rm N_2$ molecules through micropores at 77 K (Echeverria et al., 1999; Thommes et al., 2012), although QSDFT is able to improve microporosity determination (Quantachrome, 2010) in comparison with the previous version of DFT, i.e., non-local DFT (Xiao and Pignatello, 2015a, 2016) (see Fig. S1 of the Supplementary data). The zeta potential of char was measured using Zetasizer Nano-Zs analyzer (Malvern Instrument Ltd., Malvern, United Kingdom). Char samples were also characterized by Fourier transform infrared (FTIR) spectroscopy using a Nicolet iS5 spectrometer with iD5 ATR accessory (Thermo Scietific, Madison, WI, USA). Thirty-four scans were taken for each sample in the frequency range 4000–550 cm $^{-1}$ at 4 cm $^{-1}$ resolution in the transmittance mode.

Adsorption experiments of organic compounds were performed by the batch method at 22 \pm 0.5 °C and at pH of 7.1–7.4 adjusted with 0.1 mol/L HCl and NaOH. The adsorbates include two triazine herbicides (atrazine, p $K_a = 1.7$, log $K_{ow} = 2.61$; prometon, p $K_a = 4.3$, log $K_{ow} = 4.3$ 2.99) and one natural estrogen (estriol, p $K_a = 10.5$, log $K_{ow} = 2.45$) that were purchased from Sigma-Aldrich (purity: atrazine, >98%; prometon, 99%; estriol, >97%). The triazine herbicides, especially atrazine, are among the most heavily used herbicides in the U.S. and frequently detected in streams and groundwater (Gilliom, 2007; Reilly et al., 2012). Estriol is one of the most commonly detected natural estrogens in surface water (Kolpin et al., 2002; Kim et al., 2007; Velicu and Suri, 2009). The values of pK_a and $log K_{ow}$ are from Syracuse Research Corporation (SRC, 2017). The adsorbents included the original, anoxically-generated CB as well as PPAO-treated CB. The solid-to-liquid ratio was adjusted to achieve 20-75% adsorption when the uptake leveled off. The adsorption equilibrium time (7 d) was chosen on the basis of separate kinetic tests (Fig. S2 of the Supplementary data) to be sufficient to reach apparent equilibrium. After adsorption, the aqueous phase was sampled and microfiltered (0.45 µm cellulose ester filter). Adsorbate concentrations in the filtrate were determined by high performance liquid chromatography (HPLC, Agilent 1100, Santa Clara, CA) with external standards. The adsorption isotherms were fit to the Freundlich model:

$$C_{s} = K_{F}(C_{w})^{n} \tag{2}$$

where C_s and C_w are the adsorbed and aqueous-phase concentrations, respectively; n is the Freundlich exponent providing an indication of isotherm nonlinearity; and K_F ($mg^{1} - {}^nL^nkg^{-1}$) is the Freundlich adsorption coefficient. The parameters were obtained by non-linear least-squares regression weighted by the dependent variable. The observed distribution ratio (K_d , L/kg) is defined as the adsorbed-to-solution concentration ratio:

$$K_{\rm d} = \frac{C_{\rm s}}{C_{\rm w}} \tag{3}$$

The K_d is related to K_F by

$$K_{d} = K_{F}(C_{w})^{n-1} \tag{4}$$

3. Results and discussion

3.1. Burn-off of corncob char during pyrolysis, PPAO, and AP

The yield of CB from corncob during pyrolysis ranged from 25 to 43% depending on HTT (Fig. S3 of the Supplementary data), in agreement with reported yields in the literature (Zhao et al., 2013; Budai et al., 2014). Weight loss of CB particles during PPAO was determined. Depending on the carbonization HTT and PPAO temperature, the burn-

off of CB ranged from 5 to 65%, and increased with PPAO time (Fig. 1). As expected, the burn-off of partially carbonized CB samples (CB300 and CB400) was much greater than that of the higher-HTT CBs (e.g., CB600 or CB700) (Fig. 1). The effect of HTT on the burn-off during PPAO was insignificant when HTT was ≥500 °C (Fig. 1). Loss of mass during AP treatment of corncob for 0.5-h AP was 39% at 300 °C and 63% at 400 °C; the loss was ~1.5 times greater for 2-h AP.

3.2. FTIR and zeta potential measurements

As illustrated in Fig. 2, the FTIR spectrum of the original, anaerobically generated CB300 shows multiple bands at 3357–3375 (O—H stretching), 2917–2847 (C—H stretching), 2360–2159 (C=C stretching), 1791–1692 (C=C stretching, keto/aldehyde carbonyl C=O stretching, and/or carboxylic acid C=O stretching), 1590–1557 (carboxylate C=O stretching), 1433–1327 (O—H bending), 1240–1008 (C—O stretching), 951–793 (=C—H or =CH₂ bending), and 751–744 cm⁻¹ (O—H bending) (Silverstein et al., 2005; Pretsch et al., 2009; Larkin, 2011; Myneni, 2017) (Fig. 2 and Table 1). The relative intensities of the O—H stretching, O—H bending, and C=O bands increased considerably after the PPAO treatment, while the bands of C—H stretching and C=O stretching disappeared (Fig. 2 and Table 1).

The FTIR spectrum of original CB400 is similar to that of CB300, except that it shows a decrease in the C—O stretching intensity and the disappearance of the O — H stretching band. After the PPAO treatment of CB400, the C=O stretching and C—O stretching bands were markedly intensified, whereas the C—H stretching band was greatly weakened (Fig. 2 and Table 1). The O—H stretching band at 3375 cm⁻¹ also was observed on PPAO-treated CB400. Similarly, after the PPAO treatment of CB500, the relative intensities of C=O, C—O stretching, O—H bending, and O—H stretching bands increased significantly, accompanied by the disappearance of the C—H stretching band at 2879 cm⁻¹ (Fig. 2 and Table 1). The zeta potential measurements showed that 1) after PPAO treatment CB samples became more negatively charged throughout the pH range of 1.5–8; and 2) the surface negative charge density increased with increasing PPAO time (Fig. S4 of the Supplementary data). Overall, the FTIR spectra and zeta potential measurements indicate the

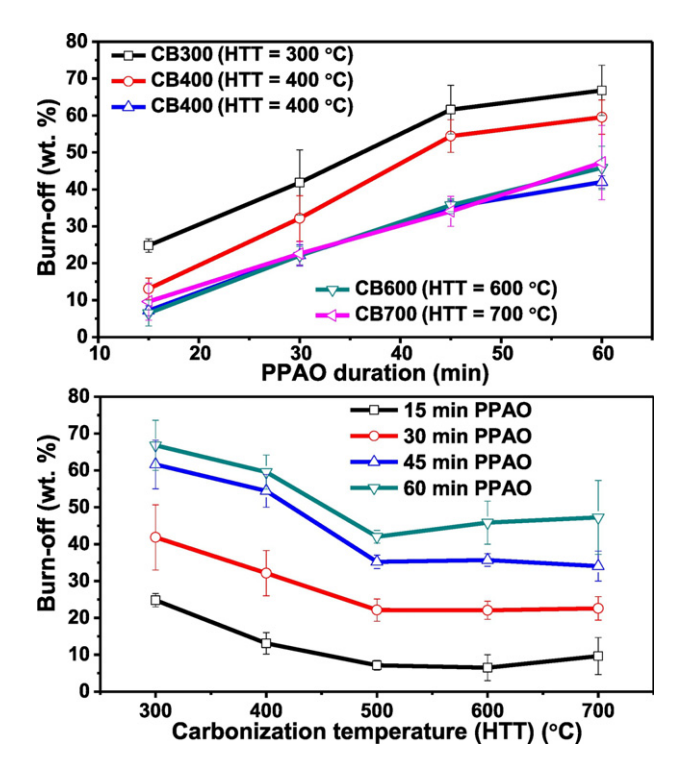


Fig. 1. Burn-off of CB samples during 15-60 min PPAO at 400 °C.

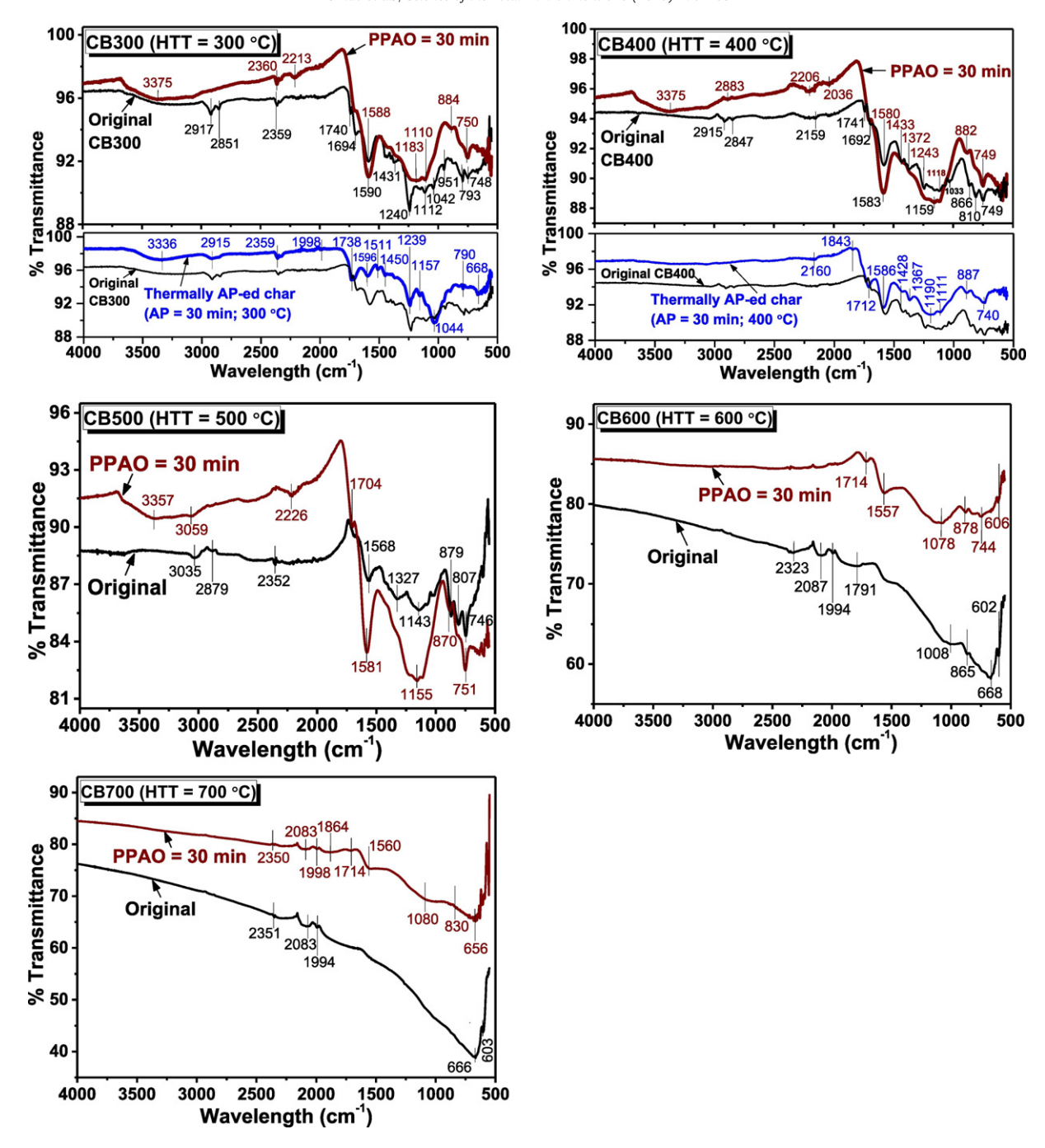


Fig. 2. FTIR spectra of anaerobically generated CB (black lines), PPAO treated (brown lines) CB, and CB made by thermal AP (blue lines).

development of surface oxygen functionality after PPAO, including dissociable acidic groups (e.g., carboxyl group), on low- or moderate-HTT (300–500 °C) chars. These results are consistent with previous potentiometric titrations showing a significant increase in surface carboxyl content after 30-min PPAO treatment of a maple wood char (Xiao and Pignatello, 2016). The oxygen-containing groups may be generated by reaction of molecular oxygen with lignocellulosic components, polyaromatic pore wall surfaces, or both.

The FTIR spectra of the char samples produced by 30-min AP at 300 and 400 °C are similar to the spectra of CB300 and CB400 produced anaerobically. A notable exception is the greater intensity of the C—O band at 1044 cm⁻¹ for the 30-min AP at 300 °C compared to the anaerobically generated CB300. Thus, thermal AP seemed not to lead to a significant generation of oxygen-containing groups on the char.

As apparent in Fig. 2, the FTIR spectra of the two well-carbonized char samples (CB600 and CB700) are very different from the spectra of CB300 and CB400. The C—O stretching and O—H stretching and bending bands were not observed in the spectra of CB600 and CB700, and the C=O stretching band was weak. The FTIR spectra of CB600 and CB700 exhibit a broad band near 666–668 cm $^{-1}$, corresponding to = C - H bending. The results suggest that high-HTT chars (CB600 and CB700) consist mainly of polyaromatic structures, in agreement with the overall conclusions of nuclear magnetic resonance spectroscopic studies (Cao et al., 2012). Notably, as shown in Fig. 2, CB600 and CB700 were deficient in surface oxygen functionality even after PPAO. For example, the bands at 1557 (C=O stretching), 1078 (C=O stretching), and 744 cm $^{-1}$ (O - H bending) were strengthened only slightly after the PPAO treatment of CB600. The zeta potential

Table 1The changes of FTIR bands of CB samples after PPAO.

The changes of Flik bands of CB samples after FFAO.			
Bands (cm ⁻¹)	Surface	Original	CB after 30-min
	functional groups	СВ	PPAO
3357-3375	O-H stretching	CB300 (med)	CB300 (stronger ^a)
			CB400 (str ^a)
			CB500 (str)
2915–2847	C—H stretching	CB300 (str)	CB400 (wk)
		CB400 (med)	
2262 2450	0.01:	CB500 (wk)	CD200 (+)
2360-2159	C≡C stretching	CB300 (str)	CB300 (str)
	of alkyne groups	CB400 (wk) CB500 (wk)	CB400 (med) CB500 (med)
		CB600 (wk)	CB500 (Inea)
		CB700 (wk)	CB700 (wk)
2087-2036	C≡C stretching	CB400 (wk)	CB400 (wk)
2007 2030	of alkyne groups	CB600 (med)	CD 100 (WK)
	or unitytic groups	CB700 (med)	CB700 (med)
1994-1992	C=C=C stretching	CB600 (wk)	()
	· ·	CB700 (wk)	CB700 (wk)
1791-1692	C=C stretching	CB300 (wk)	CB300 (wk)
		CB400 (wk)	CB400 (wk)
			CB500 (wk)
		CB600 (med)	CB600 (med)
		CB700 (wk)	CB700 (wk)
1590-1557	C=O stretching	CB300 (str)	CB300 (stronger)
		CB400 (str)	CB400 (stronger)
		CB500 (med)	CB500 (str)
		CB600 (wk)	CB600 (med)
1422 1227	0. 11 h !	CD200 (1-)	CB700 (med)
1433–1327	O—H bending	CB300 (wk)	
		CB400 (wk) CB500 (wk)	
1240-1008	C—O stretching	CB300 (wk)	CB300 (str)
1240-1008	C—O stretching	CB400 (str)	CB400 (stronger)
		CB500 (str)	CB400 (stronger)
		CB600 (wk)	CB600 (med)
		()	CB700 (med)
951-793	=C $-$ H or $=$ CH ₂	CB300 (med)	CB300 (wk)
	bending	CB400 (med)	CB400 (wk)
		CB500 (med)	CB500 (wk)
		CB600 (wk)	CB600 (wk)
751-744	O—H bending	CB300 (med)	CB300 (str)
		CB400 (str)	CB400 (str)
		CB500 (str)	CB500 (str)
			CB600 (wk)
666–668	=C-H bending in	CB600 (str)	CB700 (str)
	the polyaromatic ring	CB700 (str)	

^a Significant changes are bolded.

measurements show that CB700 became more negatively charged after PPAO, but the change in negative charge was smaller than for the low-HTT chars (Fig. S4 of the Supplementary data). In addition, burn-off during PPAO was much lower for CB600 and CB700 compared to CB300 and CB400 (Fig. 1). Overall, the results suggest that during PPAO molecular oxygen is less reactive with the well-carbonized CBs, probably due to their greater polyaromatic character.

3.3. Surface area and pore size distribution

The N_2 BET SAs of anaerobically generated CB samples increased with HTT, reaching a maximum ($40.4 \text{ m}^2/\text{g}$) at HTT of $500 \,^{\circ}\text{C}$ and then declining to $4.9 \,^{\circ}\text{m}^2/\text{g}$ at HTT of $700 \,^{\circ}\text{C}$. The BET SAs of partially carbonized CB samples (CB300 and CB400) were low ($0.5 \,^{\circ}\text{and} \, 1.4 \,^{\circ}\text{m}^2/\text{g}$, respectively). Other studies also report that the SA of biochar maximizes at HTT of $500 \,^{\circ}\text{C}$ (Lua et al., 2004; Lehmann, 2007a; Xiao and Pignatello, 2015a). The decline in SA with HTT above $500 \,^{\circ}\text{C}$ may be caused by the thermal deformation of pore structure (Lehmann and Joseph, 2009).

As illustrated in Fig. 3, PPAO treatment enhanced the BET SA of chars by up to 750 times. The SAs of all the CB samples increased significantly during the first 15 min of PPAO (Fig. 3). A more gradual increase in SA was seen during the next 15–30 min, followed by a decline in SA with longer treatment. The increase in SA can be attributed to the removal

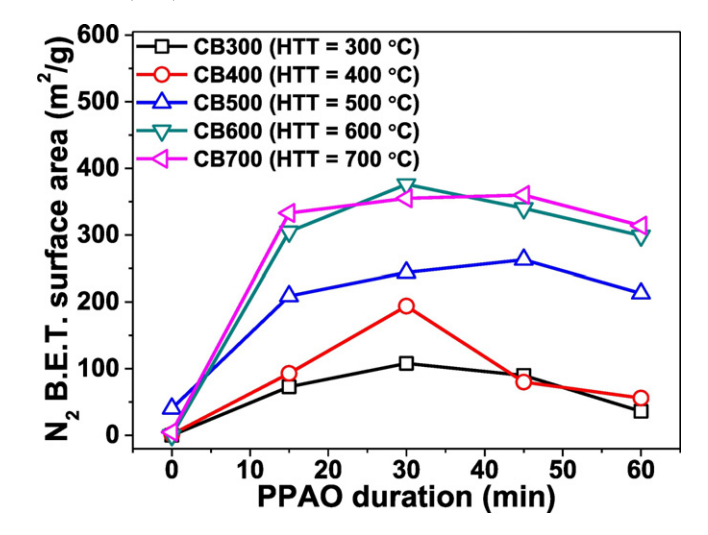


Fig. 3. Surface areas of original and PPAO treated CB samples.

of tarry matter deposited in pores during the carbonization step, or by volatilization of pore wall components; whereas, the decrease in SA with extended PPAO treatment can be attributed to thermal deformation of pore structures. Interestingly, well-carbonized chars (CB600 and CB700) experienced a greater increase in SA during PPAO than partially carbonized chars (CB300 and CB400). The SAs of thermally APgenerated char samples were below 10 m²/g and similar in magnitude to those of CB300 and CB400 (Fig. 4).

These results overall indicate that thermal air oxidation results in greater burnoff and weaker pore development for the partially carbonized chars compared to the more fully carbonized chars. The thermal reactions between molecular oxygen and uncarbonized or partially carbonized materials may contribute to partial combustion, leading to a significant weight loss (Section 3.1) and causing the degradation of newly formed pores.

The pore volume and pore size distribution of CB samples are presented in Fig. 4. The CB particles made anaerobically and by thermal AP have underdeveloped porosities, with the total porosity <0.06 cm³/g. The microporosity of CB300 and CB400, initially below 1 $\times 10^{-4}$ cm³/g, increased to 0.037 cm³/g (CB300) or 0.06 cm³/g (CB400) after 15-min PPAO. Microporosiy further increased by a factor of 1.8 with increasing PPAO time to 30 min, and then declined by a factor of ~3 to 0.024–0.034 cm³/g with longer PPAO time to 60 min. CB600 and CB700 experienced a sharp increase in microporosity after 15 min of PPAO, a slight increase from 15 to 30 min PPAO, and a slight decline with longer PPAO treatment. It is also apparent from Fig. 4 that the mesoporosity of chars, especially CB600 and CB700, also developed during PPAO. This may be due to the pore reaming effect (Xiao and Pignatello, 2016) in which molecular oxygen volatilizes carbonaceous structures along pore walls, thereby opening up pores and increasing mesoporosity. Fig. S5 of the Supplementary section presents the trends of SA and porosity as a function of burn-off during PPAO. For CB samples except CB300, SA, microporosity, and mesoporosity all maximized near 20-30 wt% of burn-off.

3.4. Adsorption isotherms

Figure S6 of the Supplementary section shows the adsorption isotherms of estriol, atrazine, and prometon on CB samples in water at pH 7.1–7.4 where the neutral form of each compound predominates. The Freundlich isotherm fitting parameters appear in Table S1 of the Supplementary section. Adsorption was nonlinear in each case, with the Freundlich nonlinearity coefficient falling in the range 0.31–0.79. Adsorption of all three compounds on the original CBs was very low. After PPAO treatment, adsorption of the three compounds increased

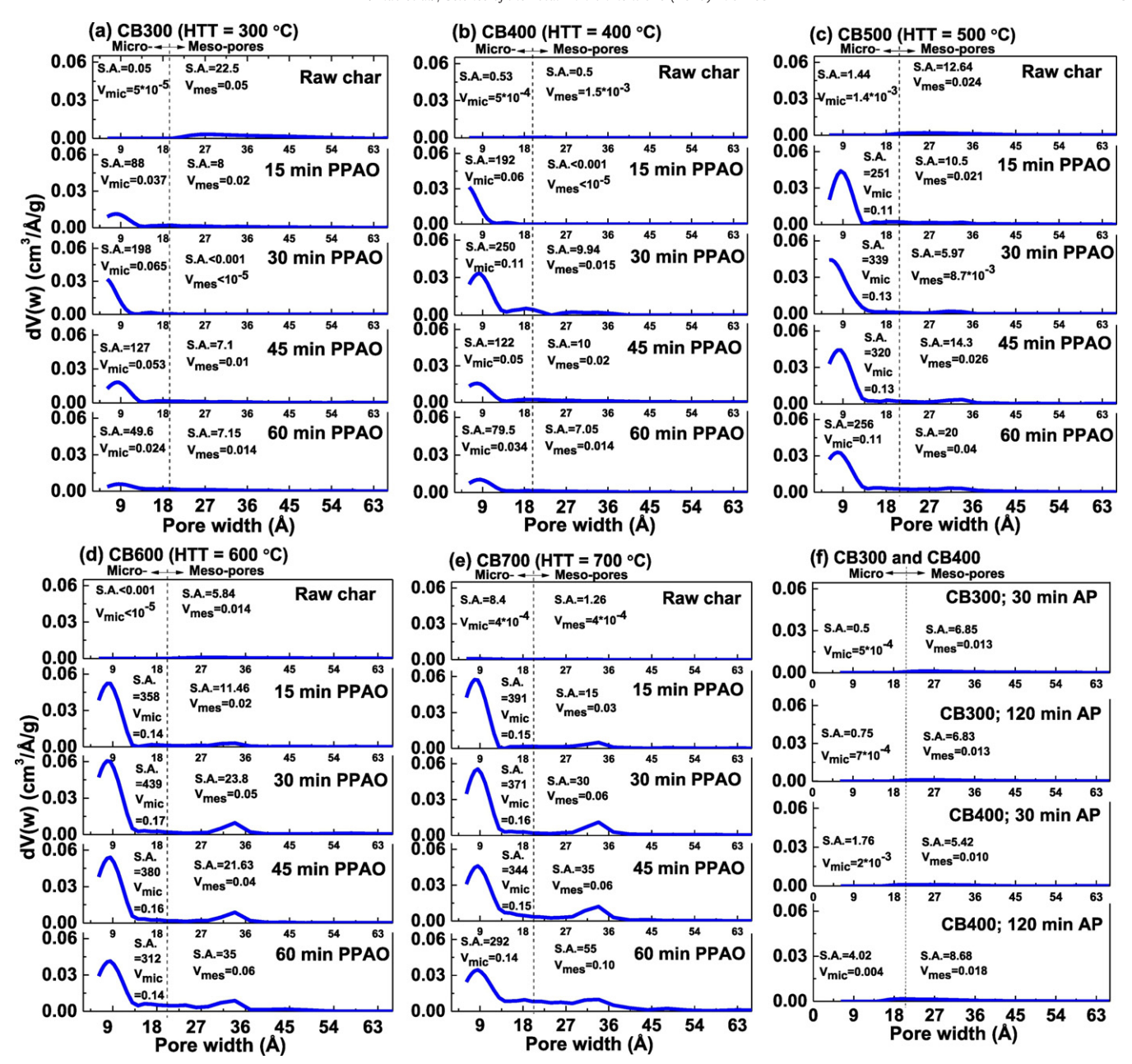


Fig. 4. Pore size distributions of anaerobically generated, PPAO treated (a-e), and thermally AP-generated (f) CB samples. The units of micro- and meso-pore volumes are cm³.

by up to 120 times depending on HTT and PPAO time. Even a brief, 15-min PPAO treatment led to a significant increase in adsorption on CB. The increase in adsorption coefficient (K_d) was greater on CB700 than on CB300 and CB400, in accord with the trends in BET SA. The increase in adsorption on CB600 and CB700 samples after PPAO may also be related to their enhanced mesoporosity (Fig. 4). Mesoporosity is thought to be important for facilitating diffusion of adsorbate molecules into micropores of char (Xiao and Pignatello, 2015a).

The physical-chemical properties of carbonaceous adsorbent that influence adsorption of neutral organic species include SA, pore size distribution, and factors related to surface chemistry. In a fundamental sense, adsorption is a function of SA, yet studies have shown that adsorption to carbonaceous materials depends on the distribution of SA among pores of different sizes (Xiao and Pignatello, 2015a) as well as the surface chemistry of the adsorbent (Xiao and Pignatello, 2015b). For example, the adsorption of estriol cannot be predicted based simply on SA and porosity. For the CB300 and CB400 series, the greatest adsorption of estriol occurred on the 60-min PPAO treated char samples, despite the 30-

min PPAO treated char having the greater SA (Fig. S6 of the Supplementary section). Furthermore, in many cases, the adsorption of estriol on PPAO-treated CB samples was similar to or even greater than the adsorption of atrazine and prometon (Fig. S6 of the Supplementary section), even though estriol appears to be less hydrophobic, as predicted by $\log K_{\rm ow}$ values. The hydroxyl groups of the neutral estriol species (hydrogen donor) may have interactions with the protonated carboxyl groups of PPAO-treated CB (hydrogen acceptor), contributing the adsorption in addition to the hydrophobic effect.

To further investigate the effects of SA on the adsorption on chars, we calculated K_d values at C_w of 0.5 and 2.5 mg/L by Eq. (2) based on the Freundlich isotherm fitting parameters (Table S1 of the Supplementary data) and tested correlations between the calculated K_d and BET SA for each of the three compounds. The resulting plots in Fig. 5a and b at the two different concentrations are biphasic, showing a relatively shallow rise in K_d with SA for chars with SA below 300 m²/g, and a much sharper rise in K_d with SA above 300 m²/g. The reason for this trend is not entirely clear, but may have to do with development of

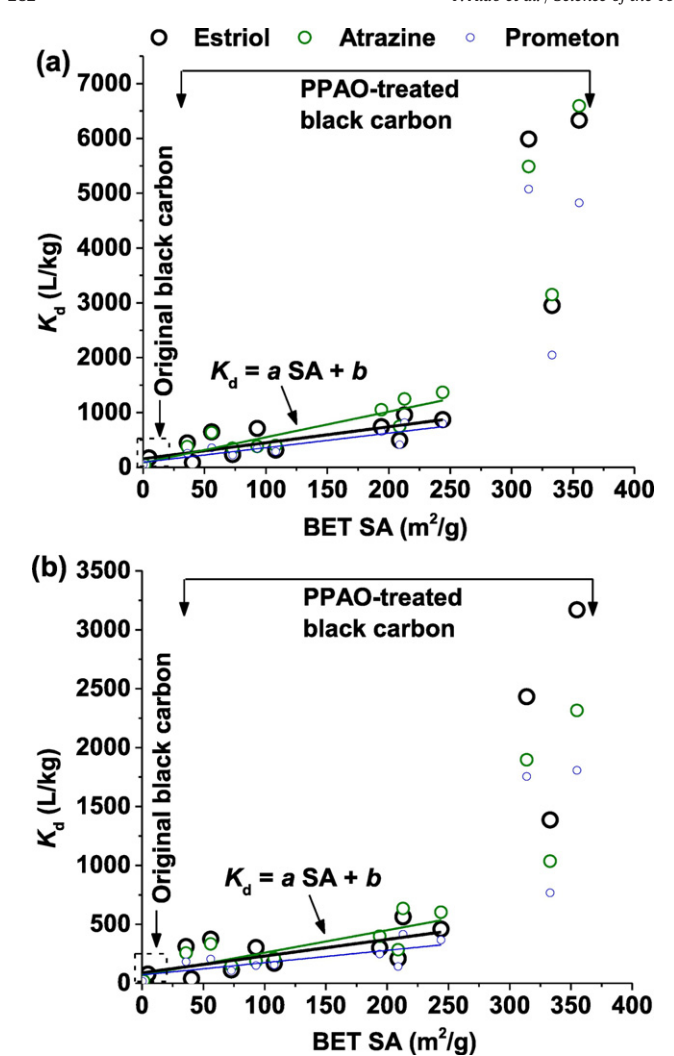


Fig. 5. Correlation between K_d and BET SA calculated at C_w of (a) 0.5 mg/L and (b) 2.5 mg/L based on the Freundlich model fits to the adsorption data (Table S1 of the Supplementary data). The lines are linear least-squares fits. At 0.5 mg/L: estriol, a=2.9, b=156.1, Pearson correlation coefficient r=0.8; atrazine, a=4.7, b=82.8, r=0.9; prometon, a=2.7, b=91.6, r=0.9. At 2.5 mg/L: estriol, a=1.4, b=88.8, r=0.7; atrazine, a=1.9, b=68.1, b=80.8; prometon, b=70.4, b=70.4, b=80.8; prometon, b=70.4, b=70.4, b=80.8; prometon, b=70.4, b=70.4,

mesoporosity during PPAO treatment. One can see by inspection of the pore size distributions in Fig. 4 that SA above about 300 m²/g is generally associated with chars that have developed significant mesoporosity as a result of PPAO treatment. The opening of new SA in the mesopore size range permits additional multilayer adsorption (i.e., pore filling), in which adsorbates condense in a liquid- or solid-like phase; whereas the opening of new SA in the micropore size range permits only additional few-layer (i.e., monolayer and bilayer) adsorption due to space limitations for the incoming molecules. Hence, a unit increase in SA in mesopores theoretically leads to a steeper increase in adsorption than a unit increase in SA in micropores. Experimentation with more compounds and more chars is needed to validate this hypothesis.

4. Conclusions

The results of this study demonstrate that thermal air oxidation can significantly affect the properties of black carbon after its formation. The results show that corncob-derived black carbon formed anaerobically or in the presence of air (thermal AP) has underdeveloped porosity and low adsorption capacity. Molecular oxygen during PPAO consumes the partially carbonized component of black carbon formed at a low HTT (300 or 400 °C), which results in a significant weight loss and a

moderate increase in SA and porosity. Well-carbonized black carbon formed at a higher HTT (600 or 700 °C) experiences a moderate weight loss during PPAO but significant increases in microporosity and mesoporosity and adsorptivity of neutral organic species. However, high-HTT black carbon after PPAO possesses much less abundant surface oxygen-containing functional groups than does low-HTT black carbon. The results also show that PPAO of black carbon can greatly enhance the adsorption of organic compounds, potentially affecting their fate and transport in soil and their bioavailability to plants and soil microorganisms. Char matter is regarded to be relatively stable with respect to decomposition in soil compared to non-pyrolytic organic matter. The results of this study indicate that char particles in the surface soil horizon that are exposed to hot air in subsequent wildfires can lose mass without disappearing completely, and their properties can be appreciably altered.

The results of this study also have practical implications for improving the performance of biochar. Amendments of PPAO treated low-HTT biochar may help increase water retention capacity of soil (Suliman et al., 2017) owing to augmentation of surface oxygen groups by PPAO. In addition, PPAO treated biochars—especially high-HTT biochars—can be effective adsorbents for removing organic compounds from water or stabilizing soils contaminated by organic compounds. Finally, char/biochar water-extractable substances have shown to be toxic to aquatic plants and animals (Smith et al., 2013; Smith et al., 2016; Wang et al., 2017b). Further studies are needed to understand the influence of thermal AO on the water-extractable toxic substances from biochar.

Acknowledgement

The authors gratefully acknowledge financial support from the University of North Dakota Pilot Postdoctoral Program (UND0021236) from the Office of Vice President for Research & Economic Development. The authors have no conflict of interest to declare.

Appendix A. Supplementary data

Supplementary data to this article can be found online at https://doi.org/10.1016/j.scitotenv.2017.11.008.

References

Amutio, M., Lopez, G., Aguado, R., Artetxe, M., Bilbao, J., Olazar, M., 2012. Kinetic study of lignocellulosic biomass oxidative pyrolysis. Fuel 95, 305–311.

Basso, A.S., Miguez, F.E., Laird, D.A., Horton, R., Westgate, M., 2012. Assessing potential of biochar for increasing water-holding capacity of sandy soils. GCB Bioenergy 5 (2), 132–143

Budai, A., Wang, L., Gronli, M., Strand, L.T., Antal Jr., M.J., Abiven, S., Dieguez-Alonso, A., Anca-Couce, A., Rasse, D.P., 2014. Surface properties and chemical composition of corncob and miscanthus biochars: effects of production temperature and method. J. Agric. Food Chem. 62 (17), 3791–3799.

Cao, X., Ma, L., Gao, B., Harris, W., 2009. Dairy-manure derived biochar effectively sorbs lead and atrazine. Environ. Sci. Technol. 43 (9), 3285–3291.

Cao, X.Y., Pignatello, J.J., Li, Y., Lattao, C., Chappell, M.A., Chen, N., Miller, L.F., Mao, J.D., 2012. Characterization of wood chars produced at different temperatures using advanced solid-state C-13 NMR spectroscopic techniques. Energy Fuel 26 (9), 5983–5991.

Chandler, C.C., Cheney, P., Thomas, P., Trabaud, L., Williams, D., 1983. Fire in Forestry. Wiley, New York.

Czimczik, C.C., Masiello, C.A., 2007. Controls on black carbon storage in soils. Global Biogeochem Cy 21, GB3005. https://doi.org/10.1029/2006GB002798.

Demirbas, 2004. Effects of temperature and particle size on bio-char yield from pyrolysis of agricultural residues. J. Anal. Appl. Sci. 72 (2), 243–248.

Echeverria, J.C., Morera, M.T., Mazkiaran, C., Garrido, J.J., 1999. Characterization of the porous structure of soils: adsorption of nitrogen (77 K) and carbon dioxide (273 K), and mercury porosimetry. Eur. J. Soil Sci. 50 (3), 497–503.

Faruk, O., Sain, M., 2016. Lignin in Polymer Composites. William Andrew/Elsevier, Kidlington, Oxford, UK; Waltham, MA, p. 15.

Gil-Lalaguna, N., Sanchez, J.L., Murillo, M.B., Ruiz, V., Gea, G., 2014. Air-steam gasification of char derived from sewage sludge pyrolysis. Comparison with the gasification of sewage sludge. Fuel 129, 147–155.

Gilliom, R.J., 2007. Pesticides in U.S. streams and groundwater. Environ. Sci. Technol. 41 (10), 3407–3413.

Glaser, B., Amelung, W., 2003. Pyrogenic carbon in native grassland soils along a climosequence in North America. Global Biogeochem Cy 17 (2).

- Glaser, B., Haumaier, L., Guggenberger, G., Zech, W., 2001. The 'Terra Preta' phenomenon: a model for sustainable agriculture in the humid tropics. Naturwissenschaften 88 (1). 37-41.
- Godlewska P. Schmidt H.P. Ok. Y.S. Oleszczuk, P. 2017. Biochar for composting improvement and contaminants reduction. A review. Bioresour. Technol. https:// doi.org/10.1016/i.biortech.2017.07.095.
- Graber, E.R., Kookana, R., 2015. In: Lehmann, J., Joseph, S. (Eds.), Biochar for Environmental Management: Science and Technology, 2nd edition.
 Graber, E.R., Tsechansky, L., Gerstl, Z., Lew, B., 2012. High surface area biochar negatively
- impacts herbicide efficacy. Plant Soil 353 (1–2), 95–106.
- III, 2017, Insurance Information Institute (III), Wildfire statistics, http://www.iii.org/factstatistic/wildfires, Accessed date: August 2017.
- Inyang, M., Gao, B., Zimmerman, A., Zhang, M., Chen, H., 2014. Synthesis, characterization, and dye sorption ability of carbon nanotube-biochar nanocomposites. Chem. Eng. J. 236, 39-46,
- Jeffery, S., Verheijen, F.G.A., van der Velde, M., Bastos, A.C., 2011, A quantitative review of the effects of biochar application to soils on crop productivity using meta-analysis. Agric. Ecosyst. Environ. 144 (1), 175-187.
- Jin, J., Sun, K., Wang, Z., Han, L., Du, P., Wang, X., Xing, B., 2017. Effects of chemical oxidation on phenanthrene sorption by grass- and manure-derived biochars. Sci. Total Environ, 598, 789-796.
- Kah, M., Sigmund, G., Hofmann, T., Hoss, S., 2017. Bioavailability and toxicity of pyrene in soils upon biochar and compost addition. Sci. Total Environ. 595, 132-140.
- Keiluweit, M., Nico, P.S., Johnson, M.G., Kleber, M., 2010. Dynamic molecular structure of plant biomass-derived black carbon (biochar). Environ. Sci. Technol. 44 (4), 1247-1253
- Kim, S.D., Cho, J., Kim, I.S., Vanderford, B.J., Snyder, S.A., 2007. Occurrence and removal of pharmaceuticals and endocrine disruptors in South Korean surface, drinking, and waste waters. Water Res. 41 (5), 1013-1021.
- Kloss, S., Zehetner, F., Dellantonio, A., Hamid, R., Ottner, F., Liedtke, V., Schwanninger, M., Gerzabek, M.H., Soja, G., 2012. Characterization of slow pyrolysis biochars: effects of feedstocks and pyrolysis temperature on biochar properties. J. Environ. Qual. 41 (4), 990–1000.
- Koelmans, A.A., Jonker, M.T., Cornelissen, G., Bucheli, T.D., Van Noort, P.C., Gustafsson, O., 2006. Black carbon: the reverse of its dark side. Chemosphere 63 (3), 365-377.
- Kolpin, D.W., Furlong, E.T., Meyer, M.T., Thurman, E.M., Zaugg, S.D., Barber, L.B., Buxton, H.T., 2002. Pharmaceuticals, hormones, and other organic wastewater contaminants in US streams, 1999-2000: a national reconnaissance. Environ. Sci. Technol. 36 (6), 1202-1211.
- Kuhlbusch, T.A.J., Crutzen, P.J., 1995. Toward a global estimate of black carbon in residues of vegetation fires representing a sink of atmospheric CO2 and a source of O2. Global Biogeochem Cy 9 (4), 491-501.
- Kupryianchyk, D., Hale, S., Zimmerman, A.R., Harvey, O., Rutherford, D., Abiven, S., Knicker, H., Schmidt, H.P., Rumpel, C., Cornelissen, G., 2016. Sorption of hydrophobic organic compounds to a diverse suite of carbonaceous materials with emphasis on biochar. Chemosphere 144, 879-887.
- Laird, D.A., 2008. The charcoal vision: a win-win-win scenario for simultaneously producing bioenergy, permanently sequestering carbon, while improving soil and water quality. Agron. J. 100 (1), 178-181.
- Larkin, P., 2011. Infrared and Raman Spectroscopy: Principles and Spectral Interpretation. Elsevier, Amsterdam, Boston, p. 1 (online resource (x, 228 pages)).
- Lehmann, J., 2007a. Bio-energy in the black. Front. Ecol. Environ. 5, 381-387.
- Lehmann, J., 2007b. A handful of carbon. Nature 447 (7141), 143-144.
- Lehmann, J., Joseph, S., 2009. Biochar for Environmental Management: Science and Technology. Earthscan Publications Ltd., London, UK.
- Lehmann, J., Joseph, S., 2015. Biochar for Environmental Management: Science, Technology and Implementation. Routledge Taylor & Francis Group, London, New York.
- Li, F., Cao, X., Zhao, L., Wang, J., Ding, Z., 2014. Effects of mineral additives on biochar formation: carbon retention, stability, and properties. Environ. Sci. Technol. 48 (19), 11211-11217.
- Lua, A.C., Yang, T., Guo, J., 2004. Effects of pyrolysis conditions on the properties of activated carbons prepared from pistachio-nut shells. J. Anal. Appl. Pyrolysis 72 (2),
- Mahinpey, N., Murugan, P., Mani, T., Raina, R., 2009. Analysis of bio-oil, biogas, and biochar from pressurized pyrolysis of wheat straw using a tubular reactor. Energy Fuel 23,
- Mao, J.D., Johnson, R.L., Lehmann, J., Olk, D.C., Neves, E.G., Thompson, M.L., Schmidt-Rohr, K., 2012. Abundant and stable char residues in soils: implications for soil fertility and carbon sequestration. Environ. Sci. Technol. 46 (17), 9571–9576.
- Marsh, H., Rodríguez-Reinoso, F., 2006. Activated Carbon. Elsevier, Amsterdam, London. Myneni, S., 2017. Infrared spectroscopy of natural organic molecules. http:// geoweb.princeton.edu/research/geochemistry/research/organics-carboxyl.html, Accessed date: August 2017.
- Neimark, A.V., Lin, Y., Ravikovitch, P.I., Thommes, M., 2009. Quenched solid density functional theory and pore size analysis of micro-mesoporous carbons. Carbon 47 (7), 1617–1628.
- Pointner, M., Kuttner, P., Obrlik, T., Jäger, A., Kahr, H., 2014. Composition of corncobs as a substrate for fermentation of biofuels. Agron. Res. 12 (2), 391-396.
- Pretsch, E., Bühlmann, P., Badertscher, M., 2009. Structure Determination of Organic Compounds: Tables of Spectral Data. Springer, Berlin.
- Qian, L., Chen, B., Hu, D., 2013. Effective alleviation of aluminum phytotoxicity by manurederived biochar. Environ. Sci. Technol. 47 (6), 2737-2745.
- Quantachrome, 2010. Quantachrome instruments. Quenched solid state functional theory (OSDFT) for pore size analysis of disordered carbon, https://www.azom.com/ article.aspx?ArticleID=5191, Accessed date: May 2017.
- Rajapaksha, A.U., Chen, S.S., Tsang, D.C., Zhang, M., Vithanage, M., Mandal, S., Gao, B., Bolan, N.S., Ok, Y.S., 2016. Engineered/designer biochar for contaminant removal/

- immobilization from soil and water: potential and implication of biochar modification Chemosphere 148 276-291
- Reilly, T.J., Smalling, K.L., Orlando, J.L., Kuivila, K.M., 2012. Occurrence of boscalid and other selected fungicides in surface water and groundwater in three targeted use areas in the United States. Chemosphere 89 (3), 228–234.
- Ronsse, F., van Hecke, S., Dickinson, D., Prins, W., 2013, Production and characterization of slow pyrolysis biochar: influence of feedstock type and pyrolysis conditions. GCB Bioenergy 5 (2), 104-115.
- Schmidt, M.W.I., Noack, A.G., 2000. Black carbon in soils and sediments: analysis, distribution, implications, and current challenges. Global Biogeochem Cy 14 (3), 777-793.
- Schmidt, M.W.I., Skjemstad, J., Czimczik, C.I., Glaser, B., Prentice, K.M., Ge'linas, Y., Kuhlbusch, T.A.J.C., 2001. Comparative analysis of black carbon in soils. Global Biogeochem Cy 15, 163-167.
- Senneca, O., Chirone, R., Salatino, P., 2002. A thermogravimetric study of nonfossil solid fuels. 2. Oxidative pyrolysis and char combustion. Energy Fuel 16 (3), 661-668.
- Silverstein, R.M., Webster, F.X., Kiemle, D.J., 2005. Spectrometric Indentification of Organic Compounds. John Wiley, New York etc.
- Skjemstad, J.O., Taylor, J.A., Smernik, R.J., 1999. Estimation of charcoal (char) in soils. Commun. Soil Sci. Plan 30 (15-16), 2283-2298.
- Skjemstad, J.O., Reicosky, D.C., Wilts, A.R., McGowan, J.A., 2002. Charcoal carbon in U.S. agricultural soils. Soil Sci. Soc. Am. J. 66 (4), 1249-1255.
- Smith, C.R., Buzan, E.M., Lee, J.W., 2013. Potential impact of biochar water-extractable substances on environmental sustainability. ACS Sustain. Chem. Eng. 1 (1), 118-126.
- Smith, C., Hatcher, P.G., Kumar, S., Lee, J.W., 2016. Investigation into the sources of biochar water-soluble organic compounds and their potential toxicity on aquatic microorganisms. ACS Sustain. Chem. Eng. 4 (5), 2550-2558.
- Spokas, K.A., Koskinen, W.C., Baker, J.M., Reicosky, D.C., 2009. Impacts of woodchip biochar additions on greenhouse gas production and sorption/degradation of two herbicides in a Minnesota soil. Chemosphere 77 (4), 574-581.
- Spokas, K.A., Novak, J.M., Masiello, C.A., Johnson, M.G., Colosky, E.C., Ippolito, J.A., Trigo, C., 2014. Physical disintegration of biochar: an overlooked process. Environ. Sci. Tech. Let. 1, 326-332.
- SRC, 2017. SRC database. http://www.syrres.com/what-we-do/databaseforms.aspx?id=
- Stefaniuk, M., Oleszczuk, P., Rozylo, K., 2017. Co-application of sewage sludge with biochar increases disappearance of polycyclic aromatic hydrocarbons from fertilized soil in long term field experiment. Sci. Total Environ. 599-600, 854-862.
- Suliman, W., Harsh, J.B., Abu-Lail, N.I., Fortuna, A.M., Dallmeyer, I., Garcia-Perez, M., 2017. The role of biochar porosity and surface functionality in augmenting hydrologic properties of a sandy soil. Sci. Total Environ. 574, 139-147.
- Thommes, M., Cychosz, K.A., Neimark, A.V., 2012. In: Tascón, J. (Ed.), Novel Carbon Adsorbents. Elsevier, Oxford, UK.
- Uchimiya, M., Bannon, D.I., Wartelle, L.H., 2012. Retention of heavy metals by carboxyl functional groups of biochars in small arms range soil. J. Agric. Food Chem. 60 (7), 1798-1809
- Velicu, M., Suri, R., 2009. Presence of steroid hormones and antibiotics in surface water of agricultural, suburban and mixed-use areas. Environ. Monit. Assess. 154 (1-4), 349-359
- Vu, T.M., Trinh, V.T., Doan, D.P., Van, H.T., Nguyen, T.V., Vigneswaran, S., Ngo, H.H., 2017. Removing ammonium from water using modified corncob-biochar. Sci. Total Environ, 579, 612-619.
- Wang, S., Gao, B., Li, Y., Creamer, A.E., He, F., 2017a. Adsorptive removal of arsenate from aqueous solutions by biochar supported zero-valent iron nanocomposite: batch and continuous flow tests. J. Hazard. Mater. 322, 172-181.
- Wang, Y., Jing, X., Li, L., Liu, W., Tong, Z., Jlang, H., 2017b. Biotoxicity evaluations of three typical biochars using a simulated system of fast pyrolytic biochar extracts on organisms of three kingdoms. ACS Sustain. Chem. Eng. 5 (1), 481–488
- Woolf, D., Amonette, J.E., Street-Perrott, F.A., Lehmann, J., Joseph, S., 2010. Sustainable biochar to mitigate global climate change. Nat. Commun. 1.
- Wu, W., Li, J., Lan, T., Muller, K., Niazi, N.K., Chen, X., Xu, S., Zheng, L., Chu, Y., Li, J., Yuan, G., Wang, H., 2017. Unraveling sorption of lead in aqueous solutions by chemically modified biochar derived from coconut fiber: a microscopic and spectroscopic investigation. Sci. Total Environ. 576, 766-774.
- Xiao, F., Pignatello, J.J., 2015a. Interactions of triazine herbicides with biochar: steric and electronic effects. Water Res. 80, 179-188.
- Xiao, F., Pignatello, J.J., 2015b. $\pi + -\pi$ interactions between (hetero)aromatic amine cations and the graphitic surfaces of pyrogenic carbonaceous materials. Environ. Sci. Technol. 49 (2), 906-914.
- Xiao, F., Pignatello, J.J., 2016. Effects of post-pyrolysis air oxidation of biomass chars on adsorption of neutral and ionizable compounds. Environ. Sci. Technol. 50 (12), 6276-6283.
- Yang, J., Zhao, Y., Ma, S., Zhu, B., Zhang, J., Zheng, C., 2016. Mercury removal by magnetic biochar derived from simultaneous activation and magnetization of sawdust, Environ. Sci. Technol. 50 (21), 12040-12047.
- Yao, Y., Gao, B., Chen, J.J., Yang, L.Y., 2013. Engineered biochar reclaiming phosphate from aqueous solutions: mechanisms and potential application as a slow-release fertilizer. Environ. Sci. Technol. 47 (15), 8700-8708.
- Zhao, X., Ouyang, W., Hao, F., Lin, C., Wang, F., Han, S., Geng, X., 2013. Properties comparison of biochars from corn straw with different pretreatment and sorption behaviour of atrazine, Bioresour, Technol, 147, 338-344.
- Zhu, X., Chen, B., Zhu, J., Xing, B., 2017. Effects and mechanisms of biochar-microbe interactions in soil improvement and pollution remediation: a review. Environ, Pollut, 227, 98-115.
- Zimmerman, A.R., 2010. Abjotic and microbial oxidation of laboratory-produced black carbon (biochar). Environ. Sci. Technol. 44 (4), 1295-1301.